Surface optical phonon propagation in defect modulated nanowires

Venkatesan, Sriram; Mancabelli, Tobia; Krogstrup, Peter; Hartschuh, Achim; Dehm, Gerhard; Scheu, Christina

Published in:
Journal of Applied Physics

DOI:
10.1063/1.4976564

Publication date:
2017

Document version
Publisher's PDF, also known as Version of record

Surface optical phonon propagation in defect modulated nanowires

Sriram Venkatesan, Tobia Mancabelli, Peter Krogstrup, Achim Hartschuh, Gerhard Dehm, and Christina Scheu

Citation: Journal of Applied Physics **121**, 085702 (2017);
View online: https://doi.org/10.1063/1.4976564
View Table of Contents: http://aip.scitation.org/toc/jap/121/8
Published by the American Institute of Physics

Surface optical phonon propagation in defect modulated nanowires

Sriram Venkatesan,[1,a)] Tobia Mancabelli,[2] Peter Krogstrup,[3] Achim Hartschuh,[2] Gerhard Dehm,[1] and Christina Scheu[1]
[1]*Max-Planck-Institut für Eisenforschung GmbH, Max-Planck-Straße 1, 40237 Düsseldorf, Germany*
[2]*Department of Chemistry and Center for NanoScience, Ludwig-Maximilians-Universität München, Butenandstr 5-13(E), 81377 München, Germany*
[3]*Center for Quantum Devices & Station Q Copenhagen, Niels Bohr Institute, University of Copenhagen, 2100 Copenhagen, Denmark*

(Received 14 October 2016; accepted 1 February 2017; published online 22 February 2017)

Planar defects, such as stacking faults and twins, are the most common defects in III–V semiconductor nanowires. Here we report on the effect of surface perturbation caused by twin planes on surface optical (SO) phonon modes. Self-catalyzed GaAs nanowires with varying planar defect density were grown by molecular beam epitaxy and investigated by Raman spectroscopy and transmission electron microscopy (TEM). SO phonon peaks have been detected, and the corresponding spatial period along the nanowire axis were measured to be 1.47 μm ($\pm$0.47 μm) and 446 nm ($\pm$35 nm) for wires with twin densities of about 0.6 ($\pm$0.2) and 2.2 ($\pm$0.18) per micron. For the wires with extremely high density of twins, no SO phonon peaks were detected. TEM analysis of the wires reveal that the average distance between the defects are in good agreement with the SO phonon spatial period determined by Raman spectroscopy. *Published by AIP Publishing.* [http://dx.doi.org/10.1063/1.4976564]

I. INTRODUCTION

Nanowires based on III–V semiconductors have attracted enormous attention owning to their application in energy conversion systems in light harvesting and nano-electronics.[1–4] GaAs is of particular interest because of its potential application in photovoltaic devices and the possibility to grow on Si as well as GaAs substrates.[5] Recently, Au free self-catalyzed GaAs nanowires were grown using molecular beam epitaxy (MBE) which allows tailoring and controlling the crystal structure and defect density.[6,7] Bulk GaAs crystallizing in cubic zinc blende (ZB) structure is the thermodynamically stable phase with a closed pack ABCABC stacking sequence along the [111] direction.[8] However, when grown as a nanowire, depending on the growth conditions like partial pressure, temperature, and catalyst droplet size, segments of hexagonal wurtzite (WZ) arrangement with the alternate stacking sequence of planes A and B along the [0001] direction can co-exist.[9] Reports also show the possibility to grow pure WZ GaAs nanowires by tuning the growth conditions.[10] The difference in the Gibbs free energies between these two crystallographic structures is small, hence the energetic barrier for nucleation of a crystal is in the same order of magnitude resulting in a polytypism.[11] This interesting behavior has a direct effect on the bandgap energies.[12] Other than stacking faults, twins are the most common defects observed in nanowires.[8,10] The defects might act as scattering regions and thus influence the electronic properties, possibly leading to a reduction in mobility and localization of the charge carriers.[13,14] It is crucial to understand the local structure and the nature of the defects in the nanowire to control properties at the nanoscale. In this work, we combine the transmission electron microscopy (TEM) and Raman optical measurements to characterise the surface defects and their density of Be-doped GaAs nanowires.

Optical spectroscopic methods for measuring transport properties in doped nanowires in a non-destructive, contactless manner are gaining popularity.[15] Raman spectroscopy is a powerful technique to measure the transport properties by exploiting the interaction between a non-zero local field associated to the longitudinal optical (LO) phonon and the charge carriers in a doped polar semiconductor. Based on this interaction, the charge carrier concentration and mobility has been successfully determined using the coupled phonon plasmon model (CPPM).[15,16] The width and the position of the Raman peaks in dependence on the charge carrier density and mobility have been characterized for n- and p-doped polar semiconductors.[17,18] The CPPM can also be generalized considering the Lindhard dielectric function[19] including Mermin's correction.[20]

In addition to the bulk transverse optical (TO) and LO modes in nanostructures, a surface optical (SO) phonon mode can exist at the interface between the nanostructure and the surrounding medium, which is of primary interest in this work. The SO mode is dominated by oscillations from the atoms located at the surface of the wire. The appearance of SO phonon modes has been predicted theoretically[21] and then observed in different nanostructures and most extensively in nanowires.[22–27] These modes can be in general observed for structures having a sufficiently high surface to volume ratio. When considering a nanowire, the morphology can be approximated as a cylinder. In this approximation, the frequency of the SO mode is[21]

$$\omega_{SO}^2 = \omega_{TO}^2 \frac{\varepsilon_s - \varepsilon_m f_\alpha}{\varepsilon_\infty - \varepsilon_m f_\alpha}, \quad (1)$$

[a)]s.venkatesan@mpie.de

where ω_{SO} is the frequency of the SO mode, ω_{TO} is the frequency of the transverse optical (TO) mode, ε_s and ε_∞ are, respectively, the static and the high frequency limit dielectric constant for GaAs. ε_m is the dielectric constant of the surrounding medium. The function f_α is given by

$$f_\alpha = -\frac{I_0(\alpha r)K_1(\alpha r)}{I_1(\alpha r)K_0(\alpha r)}. \quad (2)$$

In Equation (2), I and K are Bessel functions of the first kind for the zero and first order. The quantity α is the propagation constant of the surface oscillation. Its reciprocal $L = \frac{2\pi}{\alpha}$ represents the spatial period of SO phonon oscillation along the axial direction corresponding to the distance between the nodal points of the oscillation along the nanowire axis.[21] The aim of this work is to correlate the defects of the nanowire with this propagation constant, in order to identify the defects that cause the nodal points in the SO phonon amplitude. In handling nanostructures, phonon confinement also might play a role. The critical phonon confinement length has recently been estimated to be 23 nm for GaAs.[27] We note that the dimension of the nanowires under analysis is such that this effect can be neglected with a good approximation (see Figure 1).

The phonon propagation constant has been correlated to changes in the diameter and surface defects.[22–25] Although the SO phonon has been investigated for thin films and for nanowires, there is no systematic study revealing the direct comparison between the actual defect density to the phonon propagation constant. Here, we exploit the dependence of the SO frequency on the propagation constant of the phonon to correlate the spatial period of the oscillation along the nanowire axis with the defect characteristics of the nanowires studied by TEM. In this work, we show the excellent agreement between the twin density measured quantitatively using TEM and the spatial period L, estimated through Raman spectroscopy, which is sensitive to surface defects associated with the twins.

II. EXPERIMENTAL

The GaAs nanowires were fabricated on Si (111) substrates using a self-catalyzed vapour-liquid-solid (VLS) growth method in a Varian Gen-II molecular beam epitaxy system. We have grown three different batches of Be doped GaAs nanowires with minor changes in the growth conditions and composition. The samples are named as A, B, and C in accordance with the varying twin density in the order from the lower to the higher (see Figure 1 and below for further details). Details about the synthesis and the diffusion mechanism of the dopant can be found in a previous work.[28] Tuning the growth conditions between the growth of each batch allowed us to obtain different structural defect densities, distinct for each nanowire sample. The sample B and C belongs to the sample number 5 and 3 listed in Table I of Casadei *et al.*[28] The general growth conditions for sample A has been reported in the work of Krogstrup and co-workers.[6] The doping has no effect on the SO phonon, it influences only the LO phonon mode, and its investigation is beyond the scope of this work.

For the structural analysis, we employed a Jeol 2200 FS field emission TEM operated at 200 kV fitted with an in-column Omega filter for bright field imaging. For high resolution imaging, an aberration corrected Titan Themis 60–300 S/TEM operated at 300 kV equipped with a X-FEG source, and 4 k × 4 k CMOS-based FEI CETA camera was used. In addition to the acquired TEM images, simultaneous counting of the defects was carried out in the live imaging mode for better statistics. The nanowires are deposited on a lacy carbon TEM grid by directly scratching the Si-substrate with the grid. The measurements were carried out on 15–20 wires for each of the three different samples.

The Raman measurements are performed on an inverted microscope after deposition of the nanowires on a glass cover slide. The nanowires can be deposited on glass by drop casting after sonication in isopropanol. The nanowires are located in the sample through confocal measurements detecting the strong photoluminescence at 874 nm, corresponding to the band-gap of ZB-GaAs 1.43 eV (not shown). After the nanowires have been located, Raman spectra are measured at different positions on the same nanowires. This series of measurements is repeated at different positions on the sample. As excitation wavelength, we use the 633 nm line of a HeNe laser. The spectra are measured on an Andor Solis Sharmrock 303i spectrometer, equipped with a CCD camera Andor iDUS 420-BR-DD.

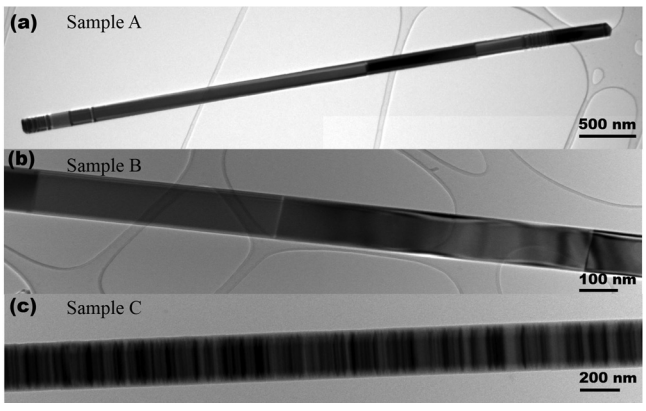

FIG. 1. Bright field TEM overview images of sample types A, B, and C showing different twin densities.

III. RESULTS AND DISCUSSION

From TEM images, the average thickness and length of the nanowires were deduced. The nanowires in sample type A are 135 nm (±15 nm) thick and 5.5 μm (±0.4 μm) long,

TABLE I. Average length and thickness of the three different sample types measured using TEM are given. The defect density is calculated as the inverse of the average spacing between defects obtained from Raman measurements (see main text for details).

Sample	Thickness (nm)	Length (μm)	Defect density (μm^{-1})
A	135 ± 15	5.5 ± 0.4	0.6 ± 0.2
B	120 ± 5	9 ± 2	(2.24 ± 0.18)
C	200 ± 25	6.5 ± 0.5	(20–100)

for the sample type B, the values are typically about 120 nm (±5 nm) and 9 μm (±2 μm) and for the sample type C 200 nm (±25 nm) and 6.5 μm (±0.5 μm). The length and thickness of the different nanowire sample types along with their defect densities is summarized in Table I. All the wires showed a constant width with slight or almost no tapering (see Figure 1). TEM observations revealed that except 1 out of 10 wires of sample type B (containing 1 unit of WZ), all others were solely composed of cubic ZB structure grown along [111] (see Figure 2). To have a WZ structure in ZB segments, two consecutive twin planes (i.e., a twin plane for every alternating monolayer) or two stacking faults are required to alter the stacking sequence from ABCABC to ABCA | C | A (where CACA forms the WZ structure) along the growth direction. However, single twins were most commonly observed in these wires.

In addition to single twins, paired twins were also observed. We use the term paired twin, when a twin follows in the vicinity (few monolayers apart) of the random single twin as described by Algra *et al.*[29] The general feature in sample types A and B is that a small region in the beginning and at the end of the wire is more heavily twinned than the major portion of the wire. The wires adopted [011] and [110] ZB orientations perpendicular to the growth direction with the paired twin region in the middle (see Figure 2(b)). The additional spots visible in the fast Fourier transform shown in the inset of Figure 2(b) indicate the presence of twins. For statistical purposes, we considered the paired twin (i.e., a twin lamella) as a single defect, and the twin distances were measured using the line intercept method from the TEM images. The paired twin forms a zig-zag pattern which causes a perturbation on the surface of the wire (see inset of Figure 2(b)). The twin plane changes the crystal orientation, because the ZB is only three fold symmetric around the nanowire axis, whereas a regular stacking fault in WZ does not change the structure because of its six fold symmetric nature. So we expect that twin planes have the largest damping effect for the phonons due to the resulting surface perturbation.

We expect that the dominating contribution to the Raman signal stems from the mid-section of the wire. First because it represents the largest part of the wire itself. Second, and more importantly, because the terminating parts have much higher defect concentrations, which prevent the observation of SO phonons (see the discussion below on sample type C). For these reasons, we focus our attention on the structure of the middle section of the wire. Careful TEM analysis reveals that the distance between twins and their corresponding surface perturbation in the different sample types are different. We measured the length of the twin free segments (as seen in Figures 1(a)–1(c)), i.e., the average distance between defects that could either be single twins or paired twins. For sample type A, a small fraction of twin defects was observed, and the average distance between them was measured to be 1.6 μm (±0.5 μm). Nanowires in sample B reveal the presence of a higher number of twins compared to the wires in sample type A. The average distance between them was measured to be 600 nm (±100 nm). The wires in sample type C that have a larger diameter were heavily twinned and a substantially smaller average twin spacing of 10–50 nm was observed. Raman spectra were measured for all the three sample types with primary interests to study the associated SO phonon mode for variable defect densities. We have simulated several spectra for all three sample types and found that the experimental data are always better reproduced when the SO phonon peak is included (except for sample C, for reasons we explain below). The SO frequency is extracted from the simulation of different Raman spectra. The propagation constant is determined from the experimentally extracted SO frequency according to Equation (1) considering a nanowire radius determined from the TEM data. From the propagation constant (α), the spatial period is calculated as $L = \frac{2\pi}{\alpha}$. In estimating the propagation constant, it is critical to correctly consider the dielectric constant of the surrounding medium. We can collect in backscattering geometry at an angle of 138° (corresponding to a numerical aperture of 1.4). The lateral section of the wires is hexagonal, and we can imagine that just one surface lays on the glass, corresponding to an angle of 60°. So a fraction of 0.565 of the light that we collect comes from the air-wire interface while a fraction of 0.435 comes from the glass/wire interface. For our calculation, we therefore used an effective dielectric constant $\varepsilon_{eff} = 0.565\ \varepsilon_{air} + 0.435\ \varepsilon_{glass}$.

A typical Raman spectrum for the wires of sample type A with a low defect density is given in Figure 3. The peaks

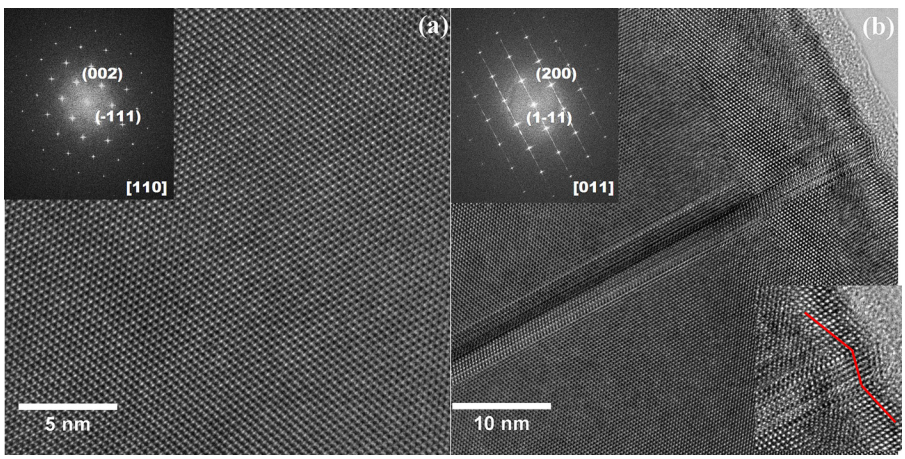

FIG. 2. High resolution TEM images showing (a) twin free segment and (b) paired twin segment of a wire from sample type B and their corresponding fast Fourier transformation is shown as the inset. The inset in the right corner of figure (b) shows the zig zag feature at the surface due to the presence of a paired twin.

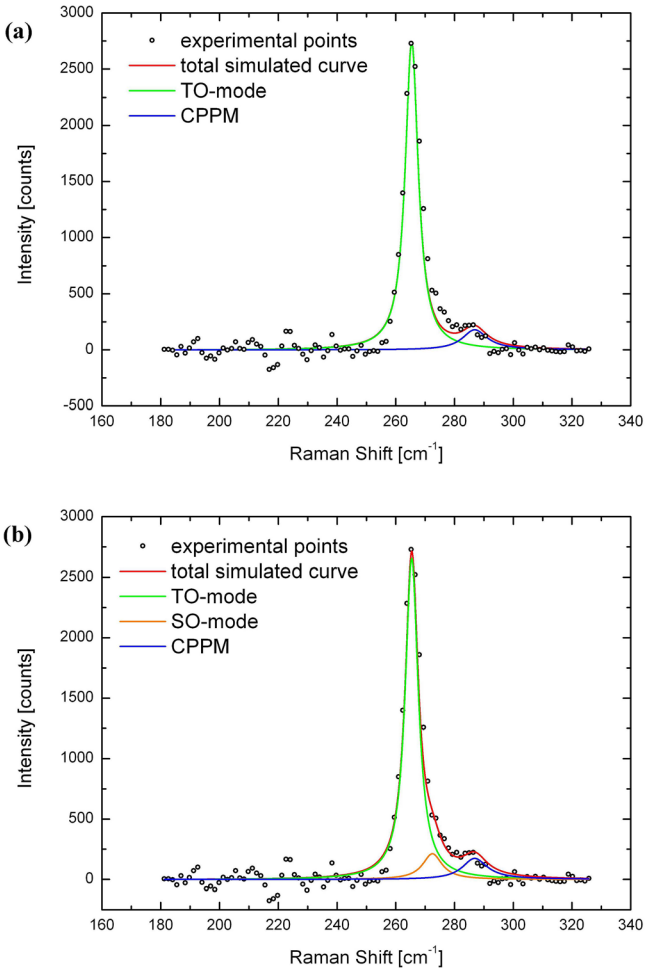

FIG. 3. Typical Raman spectrum of the sample type A showing the TO mode and CPPM. (a) The experimental spectrum was simulated without including a SO phonon peak. (b) Shows a spectrum with a SO phonon peak included in the simulation centered at 273.5 cm^{-1}.

at a frequency around 266 cm^{-1} and 288 cm^{-1} correspond to the TO and CPPM phonon mode, respectively. For the simulation of the CPPM peak, we follow the description given by Irmer and co-workers.[16–18] In this description, the dielectric function of the polar doped semiconductor is composed summing the susceptibility of the phonon and the charge carrier subsystems. For the susceptibility of the charge carriers, the classical one derived from the Drude model is taken. This formulation has been recently used to estimate the charge carrier mobility and concentration in Si-doped GaAs NWs.[15] Alternatively, one can take for the susceptibility of the charge carriers subsystem the Lindhard susceptibility[19] including Mermin's correction.[20] This description has been used to simulate the Raman spectra of n-doped GaAs NWs.[30,31] For a Raman process, the electron wave-vector is confined to small values because of the wave-vector conservation. Also, for p-doped GaAs, the hole mobility is low compared to that of electrons, which lead to a high plasma damping factor. In this regime, the descriptions based on the Drude and on the Lindhard dielectric constant coincide.[32]

We have simulated the spectra with and without including the SO phonon peak as shown in Figure 3. It is obvious from the data that, including the SO phonon peak centered at 273.5 cm^{-1} allows for a better simulation of the middle part of the spectrum where the SO peak is distinctly visible and separated from the CPPM peak. According to Equation (2), such a SO frequency would correspond to a spatial period L of 1.6 μm. The SO frequency is estimated from Equation (1) considering a radius of 67.5 nm corresponding to the half of the lateral dimension of these nanowires. Repeated optical measurements on different wires belonging to this sample

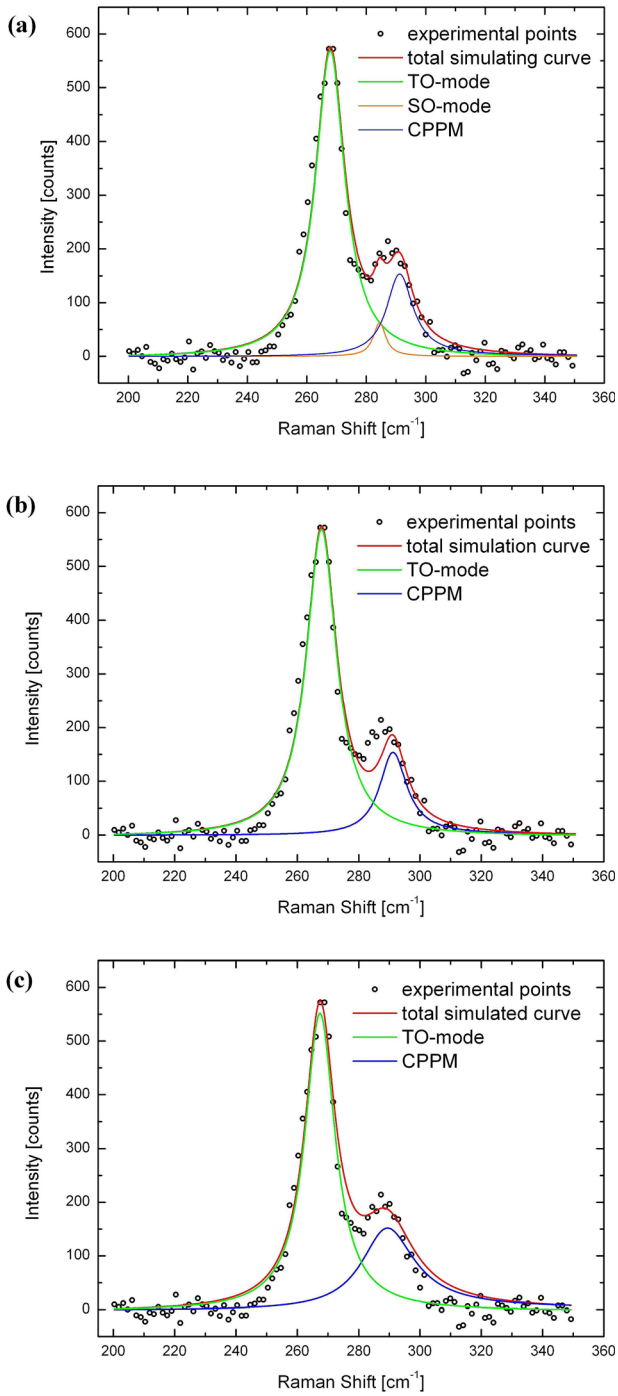

FIG. 4. Raman spectrum showing TO, SO, and CPPM peaks obtained from the sample type B. (b) and (c) show, besides the experimental data, the simulated spectra obtained without including the SO phonon peak where (a) shows the correctly simulated spectrum when the third peak is attributed to the SO phonons.

gave an average SO frequency of 274.1 cm^{-1} ($\pm$0.9 cm^{-1}), corresponding to a spatial period L of 1.47 μm ($\pm$0.47 μm) which is in close agreement to the average distance of 1.6 μm ($\pm$0.5 μm) measured between subsequent twins from TEM images.

A typical experimental Raman spectrum for the sample type B is given in Figure 4. In Figure 4(b) the spectrum where no SO phonon peak is included in the simulation to fit the experimental data shows that the CPPM peak reproduces the slope on the right side but does not reproduce the middle part of the spectrum. In Figure 4(c) the CPPM parameters are modified in order to shift the CPPM peak to a lower frequency. It is evident that, shifting the maximum of the peak to smaller energies, the slope of the peak cannot be reproduced anymore. In order to correctly simulate the spectrum as shown in Figure 4(a), one needs to include a third peak that is attributable to SO phonons, using the CPPM alone is not sufficient to correctly reproduce the shape of the second peak. From the simulation of several spectra similar to that in Figure 4, we extracted the SO-frequency for different nanowires as done for sample type A. We find a mean value of 284.3 cm^{-1} ($\pm$0.4 cm^{-1}), for the SO frequency which corresponds to a mean value of the spatial period L of 446 nm ($\pm$35 nm). The value is obtained from the propagation constant α which is estimated according to Equation (1), using a radius of 60 nm. As in the case of low twin density wires, strikingly, the value measured from the Raman spectra agrees well with the range of the average distance of 600 nm ($\pm$100 nm) between twins observed from our TEM data.

The wire type C on the other hand has a high concentration of twins (about 10–50 nm twin spacing). For this sample, we did not detect a separate SO phonon (see Figure 5). The absence of the SO phonon peak in this sample could be attributed to the high density of defects, and their SO phonon propagation translates to a very small L. In this case, the SO phonon frequency shifts to the CPPM frequency (see Figure 5) and thus cannot be distinguished. The results for all the three sample types are summarized in Table II.

The calculated SO phonon frequency as a function of the spatial period L is derived from Equation (1) for three

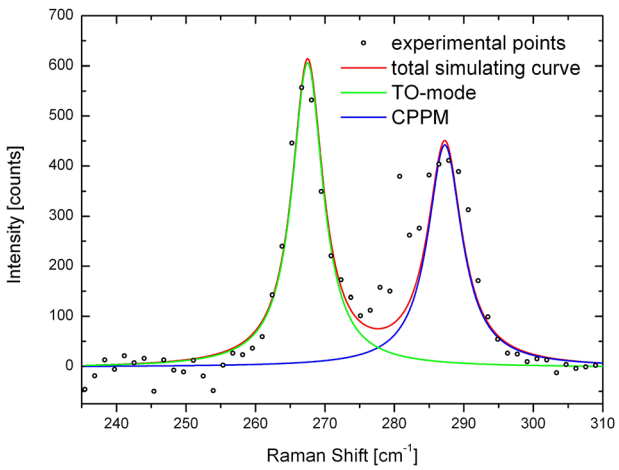

FIG. 5. Raman spectra of sample type C showing only TO and CPPM where no distinct SO phonon peaks were detected.

TABLE II. Average SO-phonon frequency (ω_{SO}) and spatial period of the phonon oscillation along the nanowire axis (L_{Raman}) extracted from the Raman spectra and calculated according to Equation (2), respectively. L_{TEM} is the average defect distance estimated by TEM.

Sample	ω_{SO} (cm^{-1})	L_{Raman} (nm)	L_{TEM} (nm)
A	274.1 $\pm$ 0.9	1470 $\pm$ 470	1600 $\pm$ 500
B	284.3 $\pm$ 0.4	446 $\pm$ 35	600 $\pm$ 100
C	Not observable	Not observable	10–50

different wire diameters as shown in Figure 6. The SO phonon frequency varies from the LO phonon frequency to the TO phonon frequency (upper and lower dashed line, respectively). The circles indicate the values for the SO phonon frequency corresponding to the estimated spatial period of the SO-phonon oscillation along the nanowire axis in the three different sample types. Each curve is calculated taking into account that the nanowires belonging to the three different sample types have different lateral dimensions (see above). The magenta circle and the magenta line correspond to sample type A, where an average spatial period of 1.47 μm ($\pm$0.47 μm) was estimated from Raman measurements. In this case, the calculated SO phonon frequency at around 274 cm^{-1} is very close to the TO phonon peak. Nonetheless, a SO phonon related peak is still observable as a shoulder of the TO phonon peak. The black circle and the black line correspond to sample B, where an average spatial period of 446 nm ($\pm$35 nm) leads to an observable SO phonon peak around 284 cm^{-1}. The blue circle and the blue line correspond to sample type C, for which no SO phonon peak could be detected. From TEM measurements, where the spacing between consequent defects appears to be 10–50 nm, we can assume the spatial period L to be around 30 nm in this case. The related SO phonon frequency would then be around 288 cm^{-1}, too close to the CPPM frequency to be observed as an independent peak in the Raman spectrum.

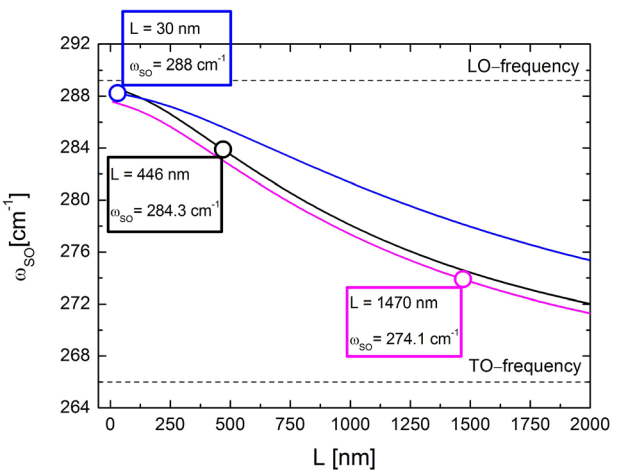

FIG. 6. The SO frequency calculated in dependence on the spatial period of surface oscillation along the axis direction according to Equation (2). The calculation is made considering the three different diameters of nanowire types A, B, and C. The circles represent a characteristic value for the SO-frequency. The lower and upper dashed black line represents the TO and LO frequency, respectively. See text for further details.

IV. CONCLUSIONS

In summary, the self catalyzed GaAs nanowires with three different defect densities were grown and analysed using TEM and Raman spectroscopy. We were able to compare the spatial period of SO phonon oscillation along the nanowire axis with the distance between the planar defects measured by TEM. This spatial period for the wires from the sample with lower defect density and moderate defect density was found to be 1.47 μm ($\pm$0.47 μm) and 446 nm ($\pm$35 nm) for the sample types A and B, respectively, which is in good agreement with the average distance between the defects, found from TEM measurements to be of about 1.6 μm ($\pm$0.5 μm) and 600 nm ($\pm$100 nm), again for sample types A and B, respectively. On the other hand, for sample type C, where no distinct Raman peak related to the SO phonons was detected, we found a defect spacing of 10–50 nm by TEM analysis. We have successfully employed the Raman spectroscopy to investigate the SO phonons which are effected by the surface perturbations induced by twins and compared to the defect density deduced using TEM. We believe that this non-destructive method of analysing the surface sensitive SO phonons provides an understanding on the structural quality of the nanowires.

ACKNOWLEDGMENTS

Authors T.M. and A.H. would like to acknowledge the support from the ERC via the starting Grant No. NEWNANOSPEC (279494) and the Deutsche Forschungsgemeinschaft (DFG) via the Cluster of Excellence Nanosystems Initiative Munich (NIM).

[1]A. I. Persson, M. W. Larsson, S. Stenstrom, B. J. Ohlsson, L. Samuelson, and L. R. Wallenberg, Nat. Mater. **3**, 677 (2004).
[2]P. Krogstrup, H. I. Jørgensen, M. Heiss, O. Demichel, J. V. Holm, M. Aagesen, J. Nygård, and A. F. I. Morral, Nat. Photonics **7**, 306 (2013).
[3]S. Gudiksen, L. Lauhon, J. Wang, D. Smith, and C. Lieber, Nature **415**, 617 (2002).
[4]C. Thelander, T. Mårtensson, M. T. Björk, B. J. Ohlsson, M. W. Larsson, L. R. Wallenberg, and L. Samuelson, Appl. Phys. Lett. **83**, 2052 (2003).
[5]V. G. Dubrovskii, T. Xu, A. D. Álvarez, S. R. Plissard, P. Caroff, F. Glas, and B. Grandidier, Nano Lett. **15**, 5580 (2015).
[6]P. Krogstrup, R. Popovitz-Biro, E. Johnson, M. H. Madsen, J. Nygård, and H. Shtrikman, Nano Lett. **10**, 4475 (2010).
[7]F. Matteini, V. G. Dubrovskii, D. Rüffer, G. Tütüncüoğlu, Y. Fontana, and A. F. I. Morral, Nanotechnology **26**, 105603 (2015).
[8]M. Koguchi, H. Kakibayashi, M. Yazawa, K. Hiruma, and T. Katsuyama, Jpn. J. Appl. Phys. **31**, 2061 (1992).
[9]D. Jacobsson, F. Panciera, J. Tersoff, M. C. Reuter, S. Lehmann, S. Hofmann, K. A. Dick, and F. M. Ross, Nature **531**, 317 (2016).
[10]P. Caroff, K. A. Dick, J. Johansson, M. E. Messing, K. Deppert, and L. Samuelson, Nat. Nanotechnol. **4**, 50 (2009).
[11]C.-Y. Yeh, Z. W. Lu, S. Froyen, and A. Zunger, Phys. Rev. B **46**, 10086 (1992).
[12]C.-Y. Yeh, S.-H. Wei, and A. Zunger, Phys. Rev. B **50**, 2715 (1994).
[13]M. D. Stiles and D. R. Hamann, Phys. Rev. B **41**, 5280 (1990).
[14]J. Wallentin, M. Ek, L. R. Wallenberg, L. Samuelson, and M. T. Borgström, Nano Lett. **12**, 151 (2012).
[15]B. Ketterer, E. Uccelli, and A. F. I. Morral, Nanoscale **4**, 1789 (2012).
[16]G. Irmer, M. Wenzel, and J. Monecke, Phys. Rev. B **56**, 9524 (1997).
[17]M. V. Klein, B. N. Ganguly, and P. J. Colwell, Phys. Rev. B **6**, 2380 (1972).
[18]G. Irmer, V. V. Toporov, B. H. Bairamov, and J. Monecke, Phys. Status Solidi B **119**, 595 (1983).
[19]J. Lindhard, Mat. Fys. Medd. Dan. Vid. Selsk **28**(14), 1–64 (1954).
[20]N. D. Mermin, Phys. Rev. B **1**, 2362 (1970).
[21]R. Ruppin and R. Englman, Rep. Prog. Phys. **33**, 149 (1970).
[22]S. Sahoo, M. S. Hu, C. W. Hsu, C. T. Wu, K. H. Chen, L. C. Chen, A. K. Arora, and S. Dhara, Appl. Phys. Lett. **93**, 233119 (2008).
[23]R. Gupta, Q. Xiong, G. D. Mahan, and P. C. Eklund, Nano Lett. **3**, 1745 (2003).
[24]D. Spirkoska, G. Abstreiter, and A. F. I. Morral, Nanotechnology **19**, 435704 (2008).
[25]N. Begum, A. S. Bhatti, F. Jabeen, S. Rubini, and F. Martelli, J. Appl. Phys. **106**, 114317–114322 (2009).
[26]P. Sahoo, S. Dhara, S. Dash, A. Tyagi, B. Raj, C. Das, P. Chandramohan, and M. Srinivasan, Int. J. Nanotechnol. **7**, 823 (2010).
[27]C. García Nuñez, A. F. Braña, J. L. Pau, D. Ghita, B. J. García, G. Shen, D. S. Wilbert, S. M. Kim, and P. Kung, J. Appl. Phys. **115**, 034307–034311 (2014).
[28]A. Casadei, P. Krogstrup, M. Heiss, J. A. Röhr, C. Colombo, T. Ruelle, S. Upadhyay, C. B. Sørensen, J. Nygård, and A. F. I. Morral, Appl. Phys. Lett. **102**, 013117–013120 (2013).
[29]R. E. Algra, M. A. Verheijen, L.-F. Feiner, G. G. W. Immink, R. Theissmann, W. J. P. van Enckevort, E. Vlieg, and E. P. A. M. Bakkers, Nano Lett. **10**, 2349 (2010), pMID: 20509677.
[30]K. S. S. Ernst, A. R. Goñi, and M. Cardona, J. Phys. Chem. Solids **56**, 567 (1995).
[31]K. S. S. Ernst, A. R. Goñi, and M. Cardona, Phys. Rev. B **50**, 1287 (1996).
[32]J. M. Ziman, *Principles of the Theory of Solis*, 2nd ed. (Cambridge University Press, 1972).